Jpn. J. Appl. Phys. Vol. 41 (2002) pp. 4571–4576
Part 1, No. 7A, July 2002

Wide-Viewing-Angle Hybrid Aligned Nematic Liquid Crystal Cell Controlled by Complex Electric Field

Seung Ho HONG[1], Hyang Yul KIM[1,3], Jae-Hyung KIM[2], Sang-Hee NAM[2], Myong-Hoon LEE[3] and Seung Hee LEE[3*]

[1]*Hyundai Display Technology, San 136-1, Ami-ri, Bubal-eub, Ichon-si, Kyungki-do 467-701, Korea*
[2]*Medical Imaging Research Center, Inje University, Kimhae, Kyungnam 621-749, Korea*
[3]*School of Advanced Materials Engineering, Chonbuk National University, Chonju-si, Chonbuk 561-756, Korea*

(Received January 18, 2002; accepted for publication April 12, 2002)

We have developed a hybrid aligned nematic liquid crystal (LC) cell driven by a complex electric field. In the device, the pixel electrode exists on the bottom substrate and the counter electrodes exist on the top and bottom substrates such that with a bias voltage both vertical and horizontal fields are generated. The LC molecules are hybrid aligned with homogeneous alignment on the bottom substrate where the alignment direction is coincident with one of the transmission axes of the crossed polarizers. Therefore, the cell appears to be black in the absence of an electric field. When a voltage is applied to obtain a white state, both vertical and horizontal fields enable the LC molecules to rotate with lowered tilt angles than those in the dark state. The device shows a much wider viewing angle than that of the twisted nematic mode, high light efficiency and low driving voltage in electro-optic characteristics. [DOI: 10.1143/JJAP.41.4571]

KEYWORDS: hybrid aligned nematic liquid crystal, complex electric field, wide viewing angle

1. Introduction

In liquid crystal displays (LCDs), the improvement of image quality and cost reduction becomes more crucial to the extension of their market and competition with other types of displays. In LCDs, the liquid crystal (LC) mode, in which initial molecular alignment and field direction are defined, mainly determines image quality and the manufacturing process of the displays. Several wide-viewing angle LC modes such as in-plane switching (IPS),[1,2] and fringe-field switching (FFS),[3–5] and multi-domain vertical alignment (MVA)[6] were developed previously. Recently, we have reported a new type of hybrid aligned nematic LCD driven by fringe-field switching (HAN-FFS) that shows a good viewing angle, high transmission and low driving voltage with a reduced number of manufacturing processes,[7,8] unlike in previous vertical-field driven HAN displays.[9,10] In the conventional HAN-FFS device, the LC molecules with negative dielectric anisotropy are initially hybrid aligned with homogenous and vertical alignments on the bottom and top substrates, respectively, and the optic axis of the LC director is coincident with one of the transmission axes of the crossed polarizers, and thus the cell appears to be black. When a voltage is applied, the fringe field that is generated by the pixel and counter electrodes existing only on the bottom substrate drives the LCs to rotate, giving rise to the bright state. In the conventional device, the LC director has a relatively high tilt angle while rotating in the fringe field. Consequently, the device needs high retardation value for maximum light efficiency, resulting in a limited viewing angle.

In order to improve the electro-optic characteristics of the HAN device driven by fringe-field switching, we have proposed a new HAN-FFS device that has common electrodes on the top substrate as well as on the bottom substrate. In this paper, simulational and experimental results, which reveal how the existence of an electrode on top substrate affects field distribution and configuration of the LC director with electro-optic characteristics are reported.

*To whom correspondence should be addressed. E-mail address: lsh1@moak.chonbuk.ac.kr

2. Simulational and Experimental Results and Discussions

Generally, in the device with uniaxial LC medium under crossed polarizers, the normalized transmission of light is

$$T/T_0 = \sin^2(2\psi)\sin^2(\pi d\Delta n/\lambda)$$

where ψ is an angle between the crossed polarizers and the LC director, and d is the cell gap, Δn is the birefringence of the liquid crystal medium, and λ is the wavelength of an incident light. Therefore, in the absence of a field, the homogeneously or hybrid aligned nematic LC cell with the optic axis coincident with one of the transmission axes of the crossed polarizers appears to be black. In the presence of a field, the LC director starts to deviate from the optic axis of crossed polarizers given the retardation of the LC medium, giving rise to transmittance; in addition, when the ψ is 45° in average, the transmission becomes maximum.

Figure 1 shows a schematic drawing of the cell structure comparing the conventional and new HAN-FFS devices with equipotential lines and configuration of the LC molecules. Here, the LC molecules are initially hybrid aligned with homogeneous alignment on the bottom surface under crossed polarizers. In the conventional HAN-FFS device, the pixel and common electrodes exist only on the bottom substrate, but in the new device, the electrode on the top substrate is connected to a common electrode on the bottom substrate, that is, the common electrodes exists on both top and bottom substrates. Consequently, a field distribution along the horizontal and vertical axes is quite different from that in the conventional one, as shown by equipotential lines. In the HAN-FFS device, the LC molecules modulate light over the whole surface area so that the pixel and common electrodes are transparent materials like indium-tin-oxides (ITOs).

The cell conditions for simulations and experiments in this paper are the same as those reported in the previous work, however, in this work, the LC with negative dielectric anisotropy ($\Delta n = 0.11$ at 589 nm, $\Delta\varepsilon = -4.7$ at 1 kHz from Merck Co.) is used and the thickness of the ITO on the top

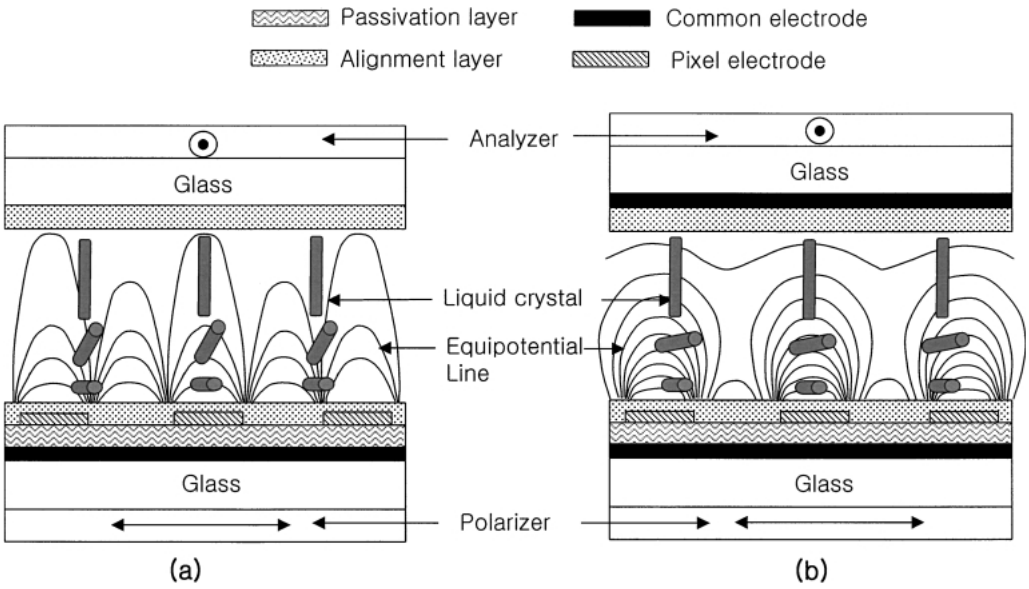

Fig. 1. Cell structures of (a) the conventional and (b) the new HAN-FFS devices with equipotential lines and configurations of the LC molecules in the white state.

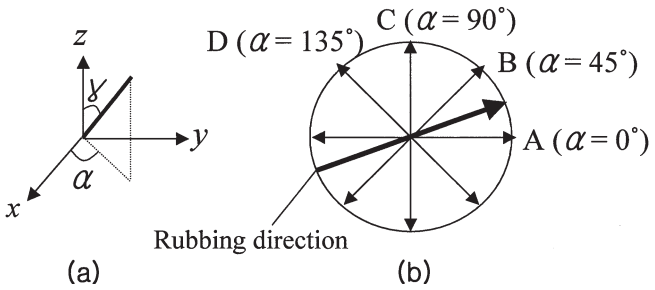

Fig. 2. (a) Definition of the viewing angle and (b) a circular coordinate showing the rubbing directions. Here A, B, C and D indicate sectional plane passing each different direction.

substrate is 1300 Å.[8] Figure 2 shows a definition of the viewing direction and circular coordinate system used in the paper. The rubbing direction was 12° with respect to y axis and A, B, C, and D indicate the sectional plane in azimuthal (α) directions passing from 0° to 180°, 45° to 225°, 90° to 270°, and 135° to 315°, respectively.

To understand electro-optic characteristics of the new device, it is necessary to understand the profile of the LC molecules corresponding to the field. For this study, we used commercially available simulation tool, LCD Master (Shintech, Japan), i.e., for field calculation the finite difference method is used, for the LC molecular alignment the continuum theory is applied and the optical transmission was obtained using 2×2 method. First, we have calculated field distribution along the horizontal axis at three different vertical distances: near the surface of the bottom substrate ($z = 0.5\,\mu$m), around the middle of the cell gap (d) ($z = 2.0\,\mu$m), and near the top surface of the upper substrate ($z = 3.5\,\mu$m). Figures 3 and 4 show the distributed field intensity of vertical (E_z) and horizontal (E_y) components

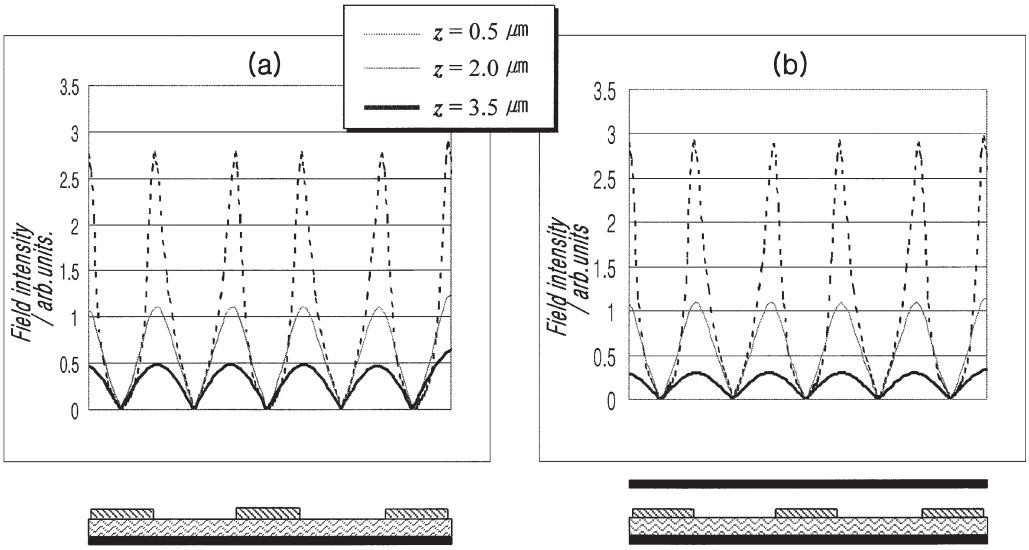

Fig. 3. Field distribution of the horizontal component in (a) the conventional and (b) the new FFS devices along the horizontal plane at several vertical distances.

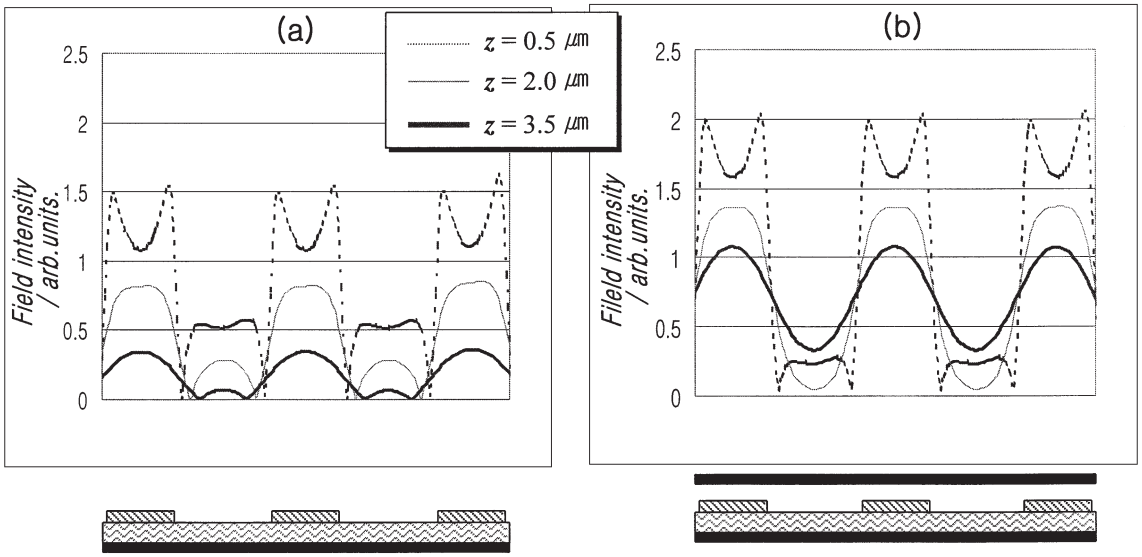

Fig. 4. Field distribution of the vertical component in (a) the conventional and (b) the new FFS devices along the horizontal plane at several vertical distances.

along a horizontal plane in the conventional and the new HAN-FFS device when a voltage of 5 V is applied. As indicated, the distribution form of E_y along horizontal axis is about the same for both devices, i.e., the field intensity of E_y around the edge of the pixel electrodes is maximum and rapidly drops to zero above the center of the electrodes, and also decreases rapidly moving away from the electrode surface to the top substrate. The maximum field intensity around the edge of the electrodes is about the same for both devices, but it is slightly weaker in the new device than in the conventional device at $z = 3.5\,\mu$m, as shown in Fig. 3. In case of E_z, the field intensities above the pixel electrode in the new device are stronger than those in the conventional device at all vertical distances; however, their maximal field intensities are weaker than E_y, as shown in Fig. 4. Such a difference in the field distribution in both devices will definitely affect the LCs to deform in different ways due to different dielectric torque. Figure 5 shows the profile of the LC molecules at a twist angle (ϕ) along the LC layers at three positions: at edge (A1), between edge and center (A2) and above the center (A3) of pixel electrodes. When a voltage of 5 V is applied, the twist angle of the LC molecules at positions A1, A2, and A3 is about the same for both devices below $z/d = 0.5$. Above mid-layer, the LC molecules are slightly more twisted in the conventional device than those in the new device at positions A1 and A2. Figure 6 shows the profile of the LC molecules in tilt angle (θ) along the LC layers at three different positions. Unlike the minor difference in the twist angle for both devices, the profile of the tilt angle shows a distinct difference between the two devices. In the conventional device, the tilt angles vary almost linearly from 2° on the low substrate to 90° on the top substrate, such that at all three positions for $z/d = 0.5$ they are close to 40°. However in the new device, for $z/d = 0.5$ at the same positions, they are much less than 40° and decreased even further down to 20° at positions A2 and A3. From these results, we can conclude that the field distributions of E_y in the two devices are not much different from each other so that the profile of the twist angle is about

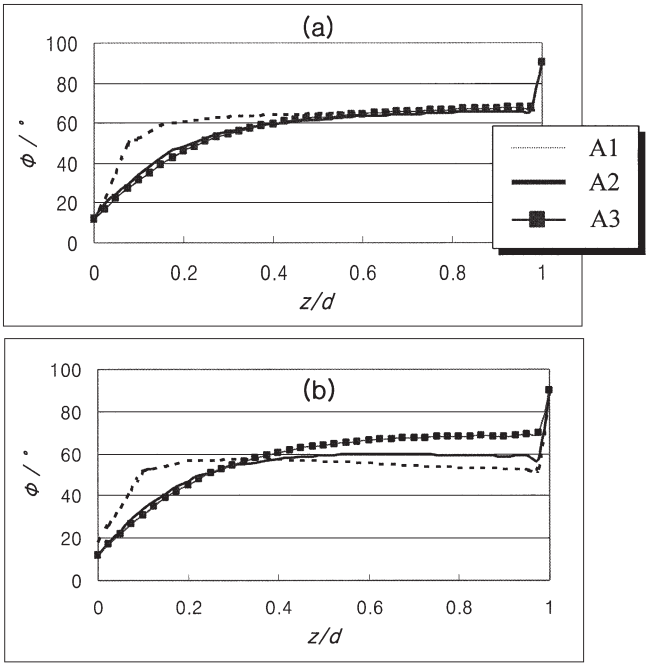

Fig. 5. Profile of the LC molecules at a twist angle along a vertical distance at three horizontal positions in (a) the conventional and (b) new HAN-FFS devices.

the same for both devices. However, the intensity of E_z above the pixel electrode becomes much stronger in the new device compared with that in the normal device and, as a result, the tilt angle of the LC molecules above the pixel electrodes decreased since the LCs with negative dielectric anisotropy orient perpendicular to the field direction.

We have calculated light transmission as a function of the retardation value of the cell in both devices by changing Δn at a fixed d, as shown in Fig. 7. The optimal retardation of the cell exhibiting maximal light efficiency is much lower for the new device than that for the conventional one. This indicates that for the new device, the LC molecules rotate with a lower tilt angle than those for the convectional device, such that the effective retardation value of the cell that gives

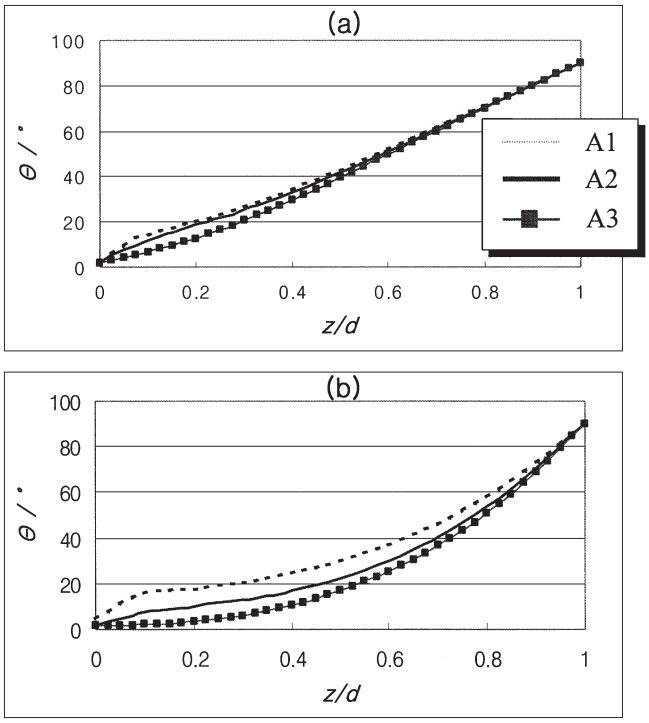

Fig. 6. Profile of the LC molecules at a tilt angle along a vertical distance at three horizontal positions in (a) the conventional and (b) new HAN-FFS devices.

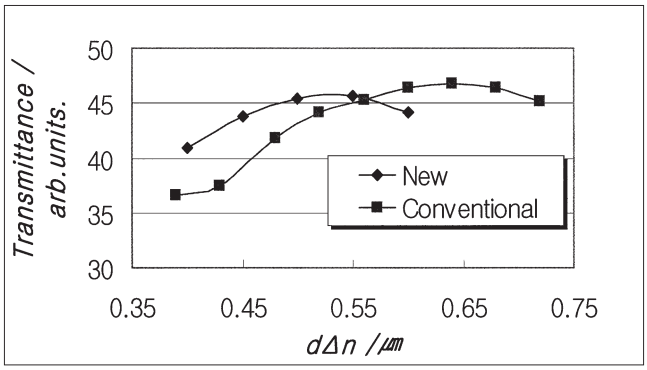

Fig. 7. Transmission as a function of retardation of the HAN-FFS cell.

rise to maximal light efficiency is decreased in the new device. In addition, both devices show light efficiency over 45% (here the light transmittance of the polarizer is assumed to be 50%). Figures 8(a) and 8(b) show calculated and experimental voltage-dependent transmission curves for both devices, respectively. Since the retardation value of the LC cell is 0.44 μm, the maximum light transmittance is higher and the driving voltage is lower for the new device than for the conventional device, which is verified through the experimental and simulational results. From these results, we conclude that the new device is advantageous in light efficiency and low driving voltage (only 3.5 V).

We have also investigated the viewing-angle characteristics of the new device and compared them with those of the conventional device. Figures 9(a) and 9(b) show the calculated and experimental viewing-angle dependency of the white state by changing polar angles (γ) up to 70° in four diagonal directions (A, B, C, D) for both devices, respectively. Both experimental and simulational results show similar trends. In the conventional device, the change rate of light transmittance from the center as the polar angle increases from right and left is not symmetric and, especially in direction B, the light transmittance increases in one direction and decreases rapidly in another direction. However, this is much improved in the new device and becomes more symmetric than what can be achieved in the conventional device. In the HAN-FFS device, as already reported in the previous paper,[8] the retardation film with retardation value $[(n_x - n_z) \cdot l = 0.2\,\mu\text{m}$ with an optic axis of 40° tilt relative to the opposite rubbing direction on the bottom substrate; l is film thickness] was used to compensate light leakage at off-normal directions. With an insertion of the retardation film between the LC cell and the top polarizer, we have calculated an iso-luminance and iso-contrast ratio up to 80° of the polar angle in all azimuthal directions with an increasing step of 10° for both devices, as shown in Figs. 10 and 11. For these simulations, the rubbing direction was assumed to be 0°. According to Fig. 10, in the conventional device the maximum transmittance does not exist at a normal direction, instead it exists at the left side of the circle (here, % indicates relative intensity to the maximum light transmittance). However, in the new device it exists at a normal direction, the uniformity in light

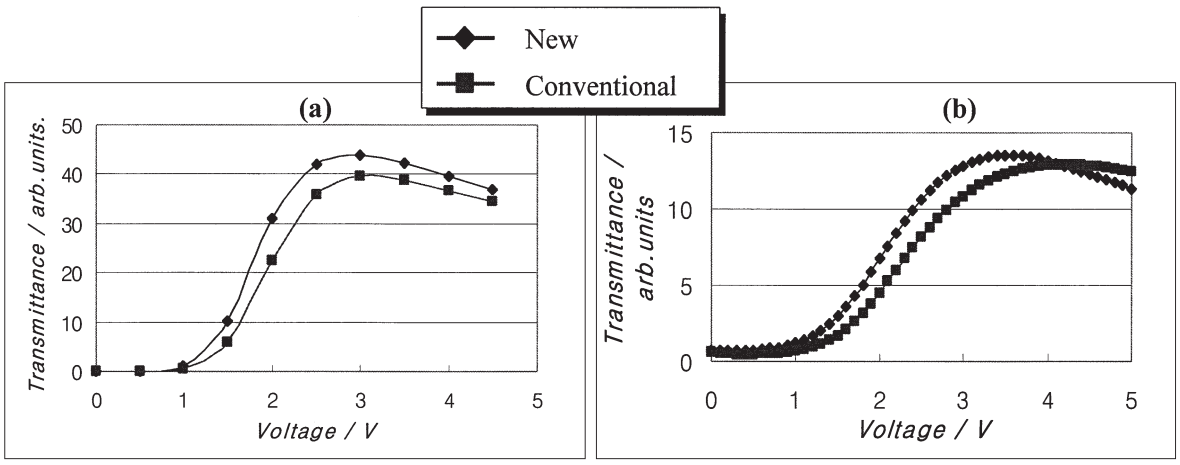

Fig. 8. (a) Calculated and (b) measured voltage-dependent transmittance in the HAN-FFS devices.

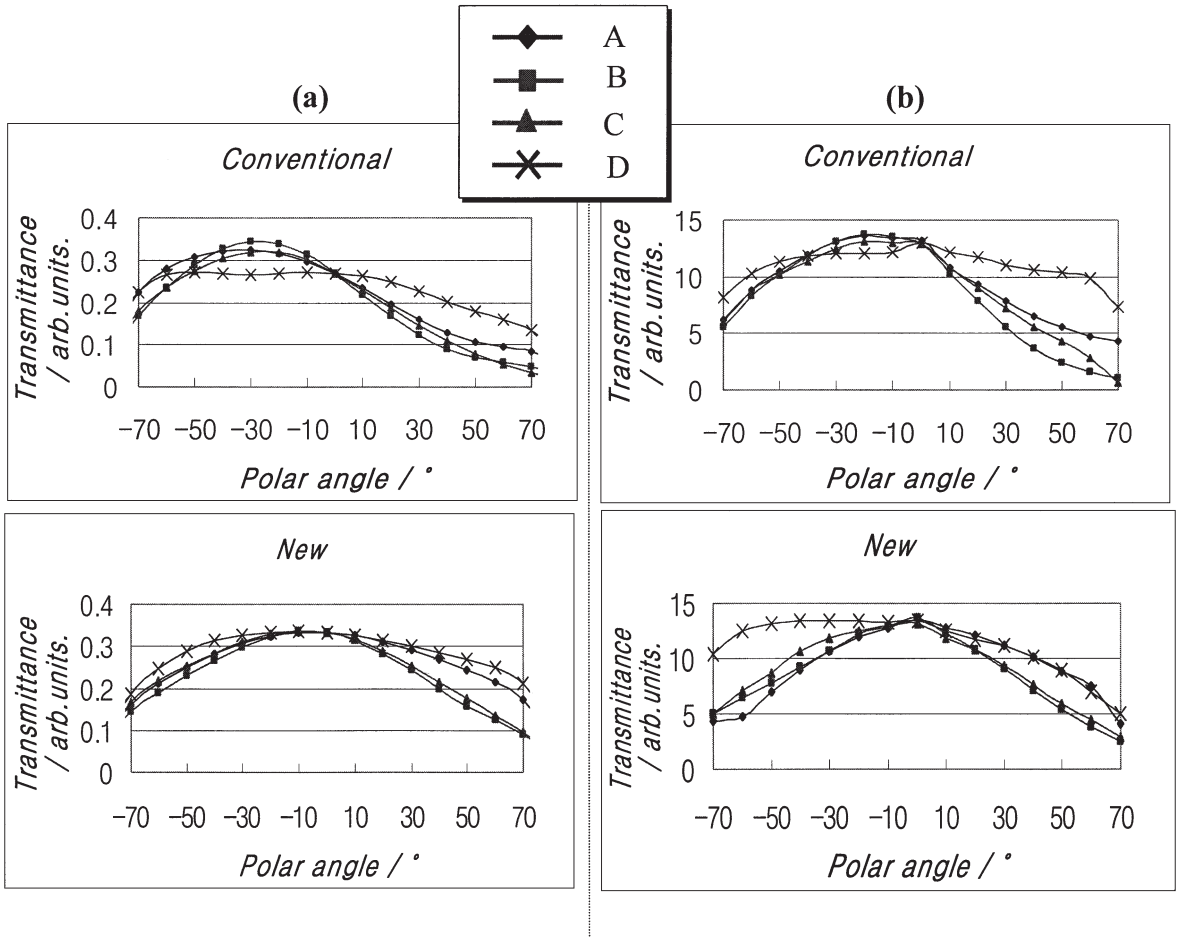

Fig. 9. (a) Calculated and (b) measured viewing-angle dependency of the white state in the conventional and the new HAN-FFS devices.

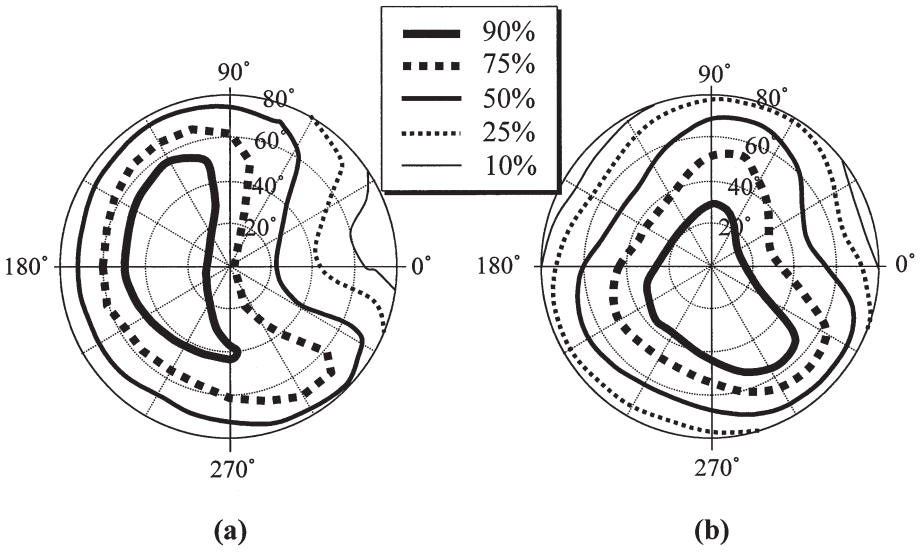

Fig. 10. Calculated iso-luminance curve of the white state in (a) the conventional and (b) the new devices.

transmittance is much improved overall and, furthermore, the region where the light intensity is about 50% exists at over a 60° polar angle in all directions. As a result, the maximum contrast ratio exists at normal directions in the new device (here, the numbers in square indicate contrast ratio), and the region where the contrast ratio is greater than 10 exists at over a 70° polar angle in all directions, as indicated in Fig. 11. In conclusion, in the new device the light uniformity is improved, and also, a viewing angle with a contrast ratio of over 10 can be achieved up to a 70° polar angle in all directions.

3. Summary

We have developed an improved HAN-FFS device and

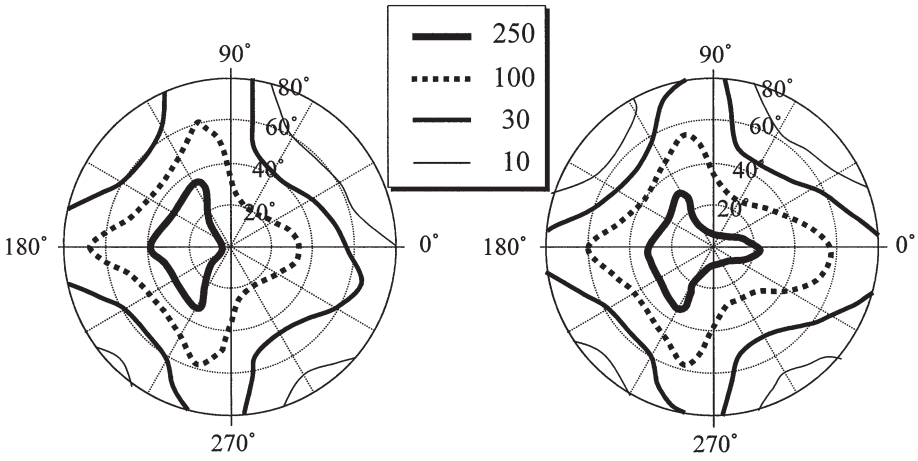

Fig. 11. Calculated iso-contrast ratio in (a) the conventional and (b) the new devices.

investigated the electro-optic characteristics of the device via experiments and simulations. The new device with common electrodes on both the top and bottom substrates enables the LC molecules to rotate with a low tilt angle, allowing the LC cell to have a low retardation value for maximal light efficiency. Consequently the new device shows very high light efficiency, low driving voltage and a wide-viewing angle with over a 70° polar angle in all directions. Furthermore, the device needs rubbing procedure performed on only one substrate, which is advantageous to the manufacturing process. We believe that the new device can be beneficially applied to both notebook computers as well as monitors.

Acknowledgement

This work was partly supported by the National Research Laboratory program (M1-10104-00-0149), Korea.

1) M. Oh-e, M. Ohta, S. Aratani and K. Kondo: Proc. 15th Int. Display Research Conf., 1995, p. 577.
2) M. Oh-e and K. Kondo: Appl Phys. Lett. **67** (1995) 3895.
3) S. H. Lee, S. L. Lee and H. Y. Kim: Appl. Phys. Lett. **73** (1998) 2881.
4) S. H. Lee, S. L. Lee and H. Y. Kim: Proc. 18th Int. Display Research Conf., 1998, p. 371.
5) S. H. Lee, S. L. Lee, H. Y. Kim and T. Y. Eom: Dig. Tech. Pap. 1999 Society for Information Display Int. Symp., 1999, p. 202.
6) A. Takeda, S. Kataoka, T. Sasaki, H. Chida, H. Tsuda, K. Ohmuro, Y. Koike, T. Sasabayashi and K. Okamoto: Dig. Tech. Pap. 1998 Society for Information Display Int. Symp., 1998 p. 1077.
7) S. H. Hong, Y. H. Jeong, K. H. Choi, H. Y. Kim, J. M. Kim, J. W. Koh and S. H. Lee: Proc. Seventh Int. Display Workshop, 2000, p. 255.
8) S. H. Hong, Y. H. Jeong, H. Y. Kim and S. H. Lee: Jpn. J. Appl. Phys. **40** (2001) L272.
9) T. Saitoh, Y. Kobayashi, Y. Iimura, S. Kobayashi, T. Hashimoto, T. Sugiyama and K. Katoh, Dig. Tech. Pap. 1996 Society for Information Display Int. Symp., 1996, p. 171.
10) Y. Tanaka, Y. Kobayashi and Y. Iimura: Proc. 5th Int. Display Workshops, 1998, p. 147.